**Featuring research from the group of Prof. Dr Jinghua Yu at the University of Jinan, Key Laboratory of Chemical Sensing & Analysis in Universities of Shandong, Jinan, China**

Flexible paper-based ZnO nanorod light-emitting diodes induced multiplexed photoelectrochemical immunoassay

ZnO nanorod inorganic/organic heterostructure light emitting diodes have been demonstrated on a cheap/disposable paper substrate, and applied in multiplexed photoelectrochemical immunoassay.

As featured in:
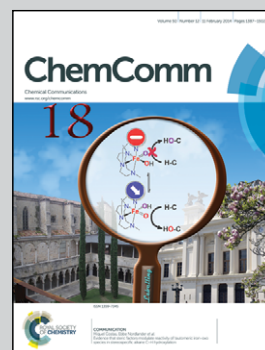
See Jinghua Yu *et al.*,
Chem. Commun., 2014, **50**, 1417.

ROYAL SOCIETY
OF **CHEMISTRY**

www.rsc.org/chemcomm

Registered charity number: 207890

ChemComm

COMMUNICATION

Flexible paper-based ZnO nanorod light-emitting diodes induced multiplexed photoelectrochemical immunoassay†

Yan Zhang,[a] Lei Ge,[a] Meng Li,[a] Mei Yan,[a] Shenguang Ge,[a] Jinghua Yu,*[a] Xianrang Song[b] and Bingqiang Cao*[c]

ZnO nanorods inorganic–organic heterostructured light-emitting diodes have been demonstrated on a cheap/disposable paper substrate and applied in multiplexed photoelectrochemical immunoassay.

Recently, flexibility of electronic devices has been found to be desirable for both manufacturing and application reasons. Taking into consideration the practical applications, as well as environmental protection, the search for portable, low-cost, smart, multifunctional and cheap electronic devices has become increasingly important. One of the most important and dominating parameters to reduce the cost is to fabricate basic electronic devices on cheap and disposable substrates like paper, which make an excellent alternative substrate for fulfilling today's commercial demands with properties different from the traditional substrate.[1] Paper, as one of the most abundant manmade materials and truly ubiquitous in modern society, has been used in recent work as a novel substrate because of its many advantages, such as being lightweight, inexpensive, foldable, renewable and biocompatible.[2] There have been some promising reports of electronic devices fabricated directly on paper substrates, such as electronic paper displays, printed circuit boards, paper super-capacitors, active-matrix organic light-emitting diodes (LEDs) and paper batteries.[3] More recently, ZnO nanostructures have also been successfully synthesized on paper substrates.[2] However, cyclotene had to be coated on the entire substrate to act as a surface barrier layer for water and other nutrient solutions, which complicated the experimental procedures.[2] Moreover, Jung and co-workers developed GaN-based LEDs on origami paper substrates with the aid of a laser lift-off process to remove the sapphire substrate, which increased the cost.[4] Inspired by this development, growth of 1D ZnO nano-structures on unmodified paper has significant importance and can

bring real breakthroughs, opening up opportunities towards flexible, lightweight, portable/wearable, biocompatible, economically cheap, and high performance functional devices. These attributes make them attractive compared to conventional stiff substrates and can induce impressive progress beyond the limits of traditional electronic and optoelectronic strategies.

Herein, we present a simple, low-cost approach to achieve portable inorganic–organic (poly(3,4-ethylenedioxythiophene)-poly(styrene sulfonate), PEDOT:PSS) heterostructured LEDs based on ZnO nanorods (NRs) on a common paper substrate (Fig. 1A).

To demonstrate the practical application of the fabricated LEDs, a carbon dots (CDs, preparation details in the ESI†) based multiplexed photoelectrochemical (PEC) immunosensor array was designed on paper-based analytical devices (Fig. 1B, fabrication details in the ESI†) using the prepared LEDs as an excitation light source (Fig. 1C). Compared with conventional PEC methods, costly light sources (cathode lamp, xenon lamp, metal halide lamp or laser) were replaced by low-cost flexible paper-based ZnO LEDs. To the best of

[a] *Key Laboratory of Chemical Sensing & Analysis in Universities of Shandong, University of Jinan, Jinan 250022, PR China. E-mail: ujn.yujh@gmail.com; Fax: +86-531-82765969; Tel: +86-531-82767161*
[b] *Cancer Research Center, Shandong Tumor Hospital, Jinan 250012, PR China*
[c] *Shandong Provincial Key Laboratory of Preparation and Measurement of Building Materials, University of Jinan, Jinan 250022, PR China. E-mail: Mse_caobq@ujn.edu.cn*
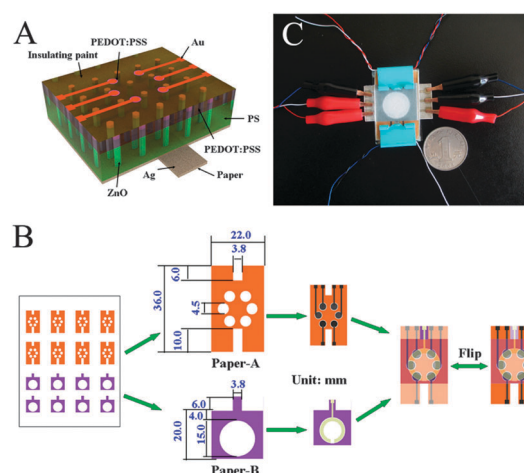† Electronic supplementary information (ESI) available. See DOI: 10.1039/c3cc48421a

Fig. 1 Schematic illustration of the (A) ZnO NRs LEDs and (B) fabricated 3D paper-based PEC devices. (C) Digital camera photograph of a paper-based ZnO NRs LEDs excited multiplexed PEC immunodevice.

our knowledge, this is the first attempt to use LED as a radiation source in PEC.

Wax was used as the paper-hydrophobization and insulation agent in the fabrication of the PEC device. Wax printing is a rapid, efficient, and inexpensive method that has been used in most applications of microfluidic paper-based analytical devices.[5] As shown in Fig. 1B, the 3D paper-based PEC device comprised of two layers of patterned rectangular papers with different sizes. The fabrication process of the wax patterns on the paper sheets can be finished within 5 min (details in the ESI†).

Finally, the wax-penetrated paper sheets were then ready for screen printing of the electrode array on their designed areas after cooling to room temperature. In addition, due to the small size of this device, the silver pads on paper-A were unnecessary and can be directly replaced by carbon ink. This will be very important for the further development of this device in low-cost applications. The six working electrodes on paper-A will share the same auxiliary electrode on paper-B once the paper PEC cell was filled with a buffer solution after stacking. The wax patterns around every electrode constituted a reservoir of the PEC cell with a volume of 10 μL on paper-A (each area) and 120 μL on paper-B.

As a principle demonstration, a self-assembly integrated electrode array was utilized to perform six-analyte immunoassay. The 3D paper-based PEC immunodevice was constructed by immobilizing the corresponding immunoarrays into the paper working zones on the back of carbon paper working electrodes (CPWEs) through sequentially assembling positively charged poly(dimethyldiallylammonium chloride) functionalized multi-walled carbon nanotubes (CNTs-PDDA) and negatively charged CDs onto the surfaces of interwoven cellulose fibers in bare paper sample zones (Fig. S5, ESI†). Briefly, 20 μL CNTs-PDDA and 20 μL CDs (photovoltaic sensitive substrates) were alternately dropped into the bare paper sample zone and kept for 10 min. After each dropping step, the paper sample zone was rinsed thoroughly according to the method demonstrated in our previous work.[5a] Finally, the capture antibodies (Ab$_1$) was immobilized into the CPWE/CNTs-PDDA/CDs through the classic N-(3-dimethylaminopropyl)-N'-ethylcarbodiimide hydrochloride (EDC) coupling reactions. Typically, a freshly prepared 15 μL solution of EDC and N-hydroxysuccinimide (NHS) were added into the CPWE/CNTs-PDDA/CDs to active the –COOH on CDs for 30 min followed by washing thoroughly with phosphate buffer solution (PBS), then 20 μL Ab$_1$ solution was dropped into the activated CPWE and then incubated at 4 °C for 4 h. Subsequently, physically absorbed excess Ab$_1$ were rinsed with PBS. Finally, the CPWE/CNTs-PDDA/CDs/Ab$_1$ was blocked by the blocking buffer for 0.5 h to cover the possible remaining active sites.

The paper substrates used in our experiments were cut from a piece of Whatman chromatography paper #2 with high flexibility. The porous structures and microfibers of the pure cellulose paper could be observed on the scanning electron microscopy (SEM) image (Fig. 2A). After screen printing the silver ink, amounts of flake structure could be observed (Fig. 2B). As a candidate substrate for the growth of ZnO NRs, the more smooth the surface the better. Therefore, an agate lapping hammer was used to polish the prepared silver electrode (Fig. 2C). Fig. 2D shows the morphology of the paper-based ZnO NRs. The hexagonal NRs have an average diameter of ∼180 nm. The
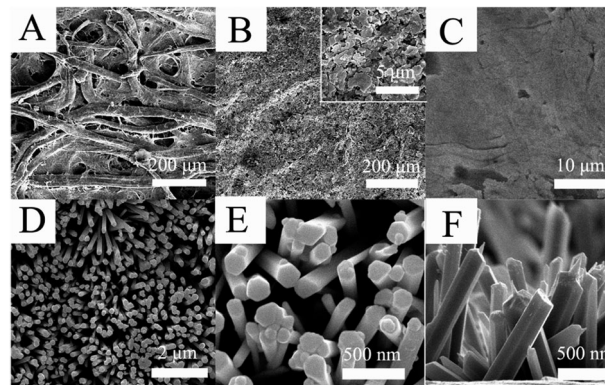

Fig. 2 SEM images of (A) pure cellulose paper, silver screen-printed paper before (B) and after (C) polishing; representative low (D) and high (E) magnification SEM images of ZnO NRs grown on paper coated with silver; (F) cross-sectional SEM image of the ZnO NRs array.

uniformity of the deposition over the complete substrate area was excellent. From the magnified SEM image (Fig. 2E), we can observe a ZnO NR array grown primarily aligned along the perpendicular direction of the paper substrate. Fig. 2F shows a cross-sectional view (90°) of the prepared ZnO paper, and it can be seen that the average height of the NRs was ∼3 μm. Furthermore, XRD and photoluminescence (PL) (Fig. 3A and B) were also used to confirm the successful preparation of ZnO NRs (details in the ESI†).

The inset in Fig. 3B shows the electroluminescence (EL) spectra of the ZnO NRs–polymer LED with the forward bias at 6 V. The EL spectrum shows emission with two peaks at 380 nm and 583 nm, respectively. The coincidence of the PL from the NRs with the shoulder in the EL spectra suggests that this transition at 380 nm is the band edge emission from the NRs. For the origin of yellow-green emission, a number of hypotheses have been proposed; it is generally accepted that the yellow-green emission is attributed to the single electron oxygen vacancy in the ZnO nanomaterials and the emission results from the radiative recombination of a photo-generated hole with an electron occupying the oxygen vacancy.[6] Meanwhile, surface states have also been identified as a possible cause of the visible emission in ZnO nanomaterials. Sun et al. have reported that surface states may play a more important role in the visible emission.[7] It is known that ZnO NRs grown using the solution method presents a large number of defects due to the nature of the method,[7] which are reflected by both PL and EL. It is possible that the surface defects contribute to the yellow-green emission. Hence, in our
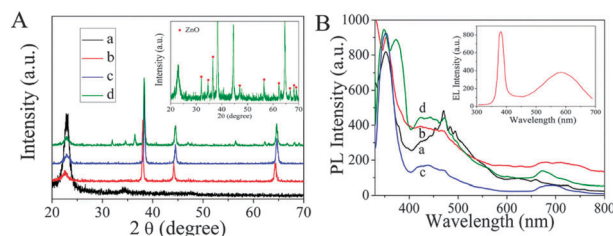

Fig. 3 (A) XRD and (B) PL spectra (λ$_{ex}$ = 315 nm) of paper (a), silver screen-printed paper (b), ZnO seed deposited paper (c) and ZnO NRs (d). The inset in (A) shows the magnified XRD spectra of ZnO NRs. The inset in (B) shows the room temperature EL spectra of ZnO NRs at applied voltages of 6 V.

case, it might be reasonably inferred that both oxygen vacancy and surface states may respond to the yellow-green emission of the prepared ZnO NRs. The band diagram of the heterostructured LED under positive bias can be found in Fig. S6 (ESI†).

Fig. S7 (ESI†) shows the current–voltage (I–V) characteristics of the fabricated ZnO NRs–polymer LED. The I–V characteristics indicate clearly that the hybrid structure exhibits a well-behaved and stable rectifying diode behavior. Stable electrical performance of hybrid devices at different bending or twisting positions is a critical challenge for flexible substrates. For this reason, we measured the mechanical fatigue properties of the diode. The inset in Fig. S7 (ESI†) shows the photograph of the folded paper substrate with large area LEDs. Interestingly, the ZnO NRs–polymer structure was still adhered and no observable changes in the I–V characteristics were seen by the rolling–bending processes (curve ii), indicating that the paper-based ZnO NRs LEDs prepared in our experiment are highly flexible and can be bent and fully recovered, which is very important for point-of-care testing (POCT).

The charge transfer and separation in photoelectrochemical immunoassay under LED irradiation could be understood as illustrated in Fig. 4A. It is speculated that the precise localization of immobilizing antigen–antibody on the individual surfaces of the multi-electrode array must be performed and the recognition of different targets must be only from different immobilized capture antibodies on each sensing electrode for multiple analysis.[8] Therefore, multiplexed PEC immunoassay between neighboring sites, several control tests including single analyte carcinoembryonic antigen (CEA), cancer antigen 125 (CA 125) or cancer antigen 15-3 (CA 15-3), two different concentrations of each and mixture of analytes (CEA + CA 125 + CA 15-3) were analyzed using the same-batch CPWEs to further monitor the cross-reactivity and cross-talk. These results (Fig. 4B) evidently supported that the cross-reactivity and cross-talk among six electrodes was negligible (details in the ESI†), which might be observed in some CCD-based high-density optical sensor arrays.[9]

To demonstrate the simultaneous quantitative immunoassays, PEC measurement was carried out after incubation with the corresponding analytes. The results (Fig. 4C–E) showed that the Δphotocurrent increased with the increase in concentration of targets and the Δphotocurrent was directly proportional to the concentration logarithm in the range 0.005–20 ng mL^{-1} for CEA, 0.01–50 U mL^{-1} for CA 125, 0.01–50 U mL^{-1} for CA 15-3. And the detection limits for the three analytes were 1.8 pg mL^{-1}, 3.6 and 3.8 mU mL^{-1}, respectively. Compared with previous studies,[10] a wider linear range and a lower detection limit were achieved with simpler steps for immunosensor fabrication. In addition, the stability and selectivity were investigated. Finally, the applicability and reliability of the proposed immunodevice for real biological samples were investigated, and showed acceptable reliability and accuracy (details can be found in the ESI†).

In summary, flexible paper-based ZnO NRs inorganic–organic heterostructured LEDs with clear rectifying behaviors were demonstrated. As a proof-of-concept, an advanced multiplexed PEC immunosensor array was fabricated using the prepared LEDs as an excitation light source, and excellent performances were obtained in real sample analysis. The combination of ZnO NRs with the low-temperature growth process can provide a significant platform for future disposable or throwaway optoelectronics. We believe that ZnO NRs on a paper substrate would be extremely useful not only in reducing production costs, but also can have many practical applications in flexible/foldable and disposable electronic devices. Furthermore, the convergence of LED technology and biotechnology opens up a new avenue for the development of simple, inexpensive, portable, and easy-to-use POCT platforms for public health, environmental monitoring in developing countries, and in resource-limited and remote regions with limited facilities.

Notes and references

1 M. Y. Soomro, S. Hussain, N. Bano, I. Hussain, O. Nur and M. Willander, *Phys. Status Solidi A*, 2013, **210**, 1600.
2 G. Amin, S. Zaman, A. Zainelabdin, O. Nur and M. Willander, *Phys. Status Solidi RRL*, 2011, **5**, 71.
3 (a) D. Graham-Rowe, *Nat. Photonics*, 2007, **1**, 248; (b) D. H. Kim, Y. S. Kim, J. Wu, Z. J. Liu, J. Z. Song, H. S. Kim, Y. G. Y. Huang, K. C. Hwang and J. A. Rogers, *Adv. Mater.*, 2009, **21**, 3703; (c) L. Ge, P. P. Wang, S. G. Ge, N. Q. Li, J. H. Yu, M. Yan and J. D. Huang, *Anal. Chem.*, 2013, **85**, 3961; (d) P. Andersson, D. Nilsson, P. O. Svensson, M. Chen, A. Malmström, T. Remonen, T. Kugler and M. Berggren, *Adv. Mater.*, 2002, **14**, 1460; (e) B. Scrosati, *Nat. Nanotechnol.*, 2007, **2**, 598.
4 Y. H. Jung, X. T. Wang, J. W. Kim, S. H. Kim, F. Ren, S. J. Pearton and J. Kim, *Appl. Phys. Lett.*, 2012, **100**, 231113.
5 (a) L. Ge, J. X. Yan, X. R. Song, M. Yan, S. G. Ge and J. H. Yu, *Biomaterials*, 2012, **33**, 1024; (b) E. Carrilho, A. W. Martinez and G. M. Whitesides, *Anal. Chem.*, 2009, **81**, 7091.
6 K. Vanheusden, W. L. Warren, C. H. Seager, D. R. Tallant, J. A. Voigt and B. E. Gnade, *J. Appl. Phys.*, 1996, **79**, 7983.
7 X. W. Sun, J. Z. Huang, J. X. Wang and Z. Xu, *Nano Lett.*, 2008, **8**, 1219.
8 (a) Y. Zhang, W. Y. Liu, S. G. Ge, M. Yan, S. W. Wang, J. H. Yu, N. Q. Li and X. R. Song, *Biosens. Bioelectron.*, 2013, **41**, 684; (b) X. Chen, X. L. Jia, J. M. Han, J. Ma and Z. F. Ma, *Biosens. Bioelectron.*, 2013, **50**, 356.
9 J. F. Ding, Y. Z. Yang and X. E. Zhang, *Gene Analysis and Biochip Technology*, Hubei Science and Technology Press, Wuhan, 1st edn, 2004.
10 (a) D. P. Tang, R. Yuan and Y. Q. Chai, *J. Phys. Chem. B*, 2006, **110**, 11640; (b) J. Wu, Z. J. Zhang, Z. F. Fu and H. X. Ju, *Biosens. Bioelectron.*, 2007, **23**, 114; (c) H. Li, J. He, S. J. Li and A. P. F. Turner, *Biosens. Bioelectron.*, 2013, **43**, 25; (d) W. W. Tu, W. J. Wang, J. P. Lei, S. Y. Deng and H. X. Ju, *Chem. Commun.*, 2012, **48**, 6535; (e) P. P. Wang, L. Ge, S. G. Ge, J. H. Yu, M. Yan and J. D. Huang, *Chem. Commun.*, 2013, **49**, 3294.
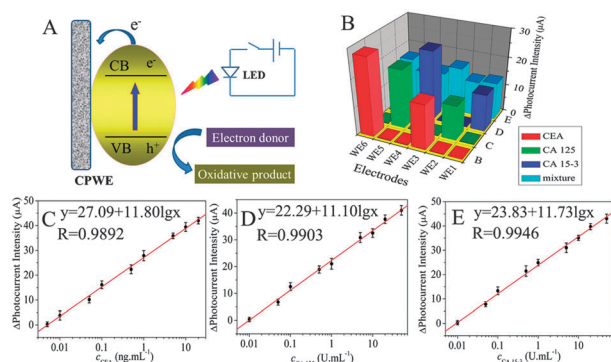
Fig. 4 (A) Schematic illustration for the charge transfer and separation. (B) ΔPhotocurrent intensity of the immunosensor array for the independent detection of tumor markers. WE1−WE6 modified with CA 15-3-Ab$_1$, CA 125-Ab$_1$, CEA-Ab$_1$, CA 15-3-Ab$_1$, CA 125-Ab$_1$, and CEA-Ab$_1$, respectively. Calibration curves (C−E) for the multiplexed PEC immunoassay tumor markers.

Electronic Supplementary Information

Flexible paper-based ZnO nanorods light-emitting diodes induced multiplexed photoelectrochemical immunoassay

Yan Zhang[a], Lei Ge[a], Meng Li[a], Mei Yan[a], Shenguang Ge[a], Jinghua Yu[a,]*, Xianrang Song[b], and Bingqiang Cao[c,]*

[a] *School of Chemistry and Chemical Engineering, University of Jinan, Jinan 250022,*

P.R. China   E-mail: ujn.yujh@gmail.com

[b] *Cancer Research Center, Shandong Tumor Hospital, Jinan 250012, P.R. China*

[c] *Shandong Provincial Key Laboratory of Preparation and Measurement of Building*

Materials, University of Jinan, Jinan 250022, P.R. China

E-mail: Mse_caobq@ujn.edu.cn

Experimental section

Materials and apparatus

All reagents were of analytical-reagent grade and directly used for the following experiments without further purification. Zinc acetate dehydrate and methenamine were obtained from Sinopharm Chemical Regent Co. Ltd (Shanghai, China). The hole-conducting polymer PEDOT:PSS was obtained from Suzhou Yacoo Corporation. Poly(dimethyldiallylammonium chloride) (PDDA, 20%, w/w in water, molecular weight = 200 000-350 000), N-(3-di-methyl-aminopropyl)-N'-ethylcarbodiimidehydro-chloride (EDC) and N-hydroxy-succinimide (NHS) were purchased from Alfa Aesar China Ltd. Multi-walled carbon nanotubes (CNTs, diameter, 30-50 nm) were purchased from Nanoport. Co. Ltd. (Shenzhen, China). Carcinoembryonic antigen (CEA), cancer antigen 125 (CA 125) and cancer antigen 15-3 (CA 15-3) standard solutions, the capture antibodies of them (CEA-Ab$_1$, CA 125-Ab$_1$, CA 15-3-Ab$_1$) were purchased from Shanghai Linc-Bio Science Co. Ltd. (Shanghai, China). Silver paste was purchased from Shanghai Jiuyin Electronic Technology Co. Ltd (Shanghai, China). Carbon ink (ED423ss) and Ag/AgCl ink (CNC-01) were purchased from Acheson. Whatman chromatography paper #2 (460.0 mm × 570.0 mm) (pure cellulose paper) was obtained from GE Healthcare Worldwide (Pudong, Shanghai, China) and used with further adjustment of size. The aqueous solutions unless indicated were prepared with ultra-pure water which was obtained from a Lichun water purification system ($\geqslant$18 MΩ·cm, Jinan, China). The clinical serum samples were provided by Shandong Tumor Hospital.

Electrochemical impedance spectroscopy (EIS) was carried out on an IM6x electrochemical station (Zahner, Germany). Impedance measurements were performed by applying an AC voltage of 5 mV amplitude in the frequency range of 0.01 Hz to 10^5 Hz in a 5 mM $[Fe(CN)_6]^{3-/4-}$ redox probe solution with 0.1 M KCl. Photoluminescence (PL) and electroluminescence (EL) spectrum were recorded on a RF-5310pc spectrofluorophotometer (Shimadzu, Japan). Scanning electron microscopy (SEM) images were obtained using a QUANTA FEG 250 thermal field emission scanning electron microscopy (FEI Co., USA). Transmission electron

microscopy (TEM) images were obtained from a JEOL JEM-1400 microscope (Japan). The phase characterization was performed by X-ray diffraction (XRD) using a D8 advance diffractometer system equipped with Cu Kα radiation (Bruker Co., Germany).

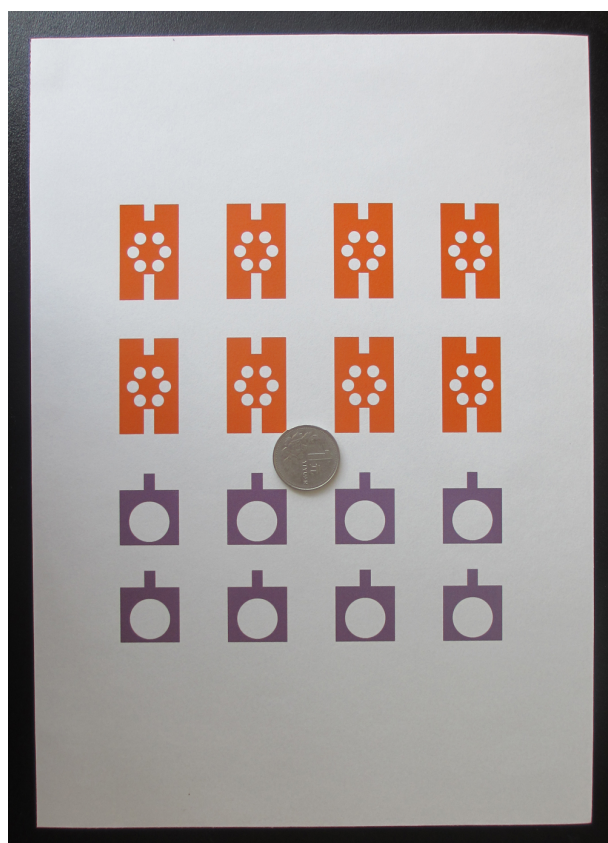**Fabrication of the 3D paper-based PEC device**

Fig. S1 Wax-printed patterns on a paper sheet (A4) before baking.

As shown in Fig. 1B, the 3D paper-based PEC device was comprised of two layers of patterned rectangular papers with different size (paper-A, 36.0 mm × 22.0 mm, and paper-B, 30.0 mm × 22.0 mm). The shape of the hydrophilic working zones was designed with Adobe illustrator CS4. On paper-A, the wax-patterns contains six working zones (4.5 mm in diameter) and corresponding conductive channels. On paper-B, there is only a circular contacting zone (15.00 mm in diameter) with a corresponding conductive channel. The fabrication process of the wax-patterns on the paper sheets was comprised of only two steps after designing the patterns on the

computer: (i) the two wax patterns were printed onto the surface of pure paper with a wax printer (FUJIXEROX Phaser 8560DN, Japan) (Fig. S1); (ii) the wax-printed paper sheets were baked in an oven at 130°C for 150 s to melt the printed wax so that it penetrated through the paper to form the hydrophobic and insulating patterns (Fig. S2). These two steps can be finished within 5 min.
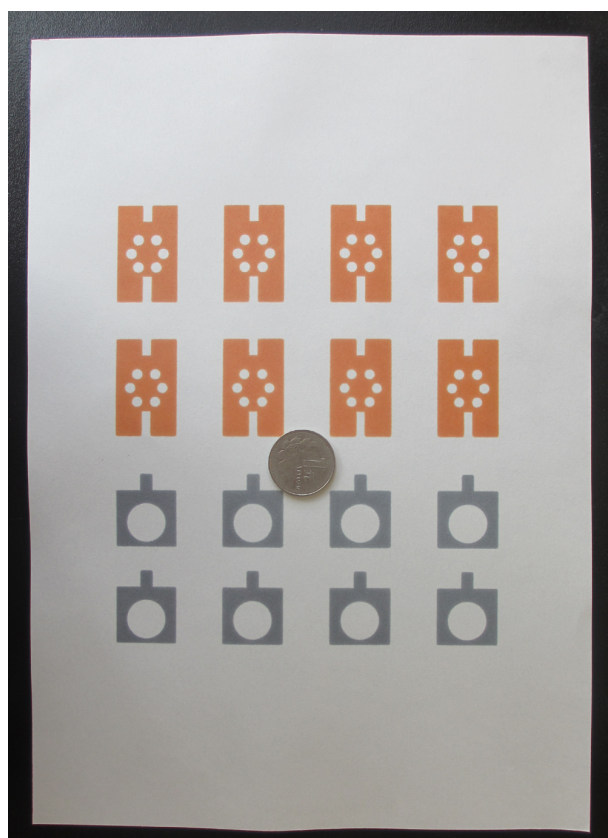

Fig. S2 Wax-printed patterns on a paper sheet (A4) after baking.

Finally, the wax-penetrated paper sheets were then ready for screen-printing of the electrode array on its designed areas after cooling to room temperature. For the upper eight patterns, six working electrodes, the wires and contact pads were screen-printed in the defined area using carbon ink (Fig. S3). For the lower eight patterns, an auxiliary electrode was screen-printed in the defined contacting zone using Ag/AgCl ink (Fig S4). After that, they were cut to paper-A and paper-B. The six working electrodes on paper-A will share the same auxiliary electrode on paper-B once the paper PEC cell was filled with buffer solution after stacking.
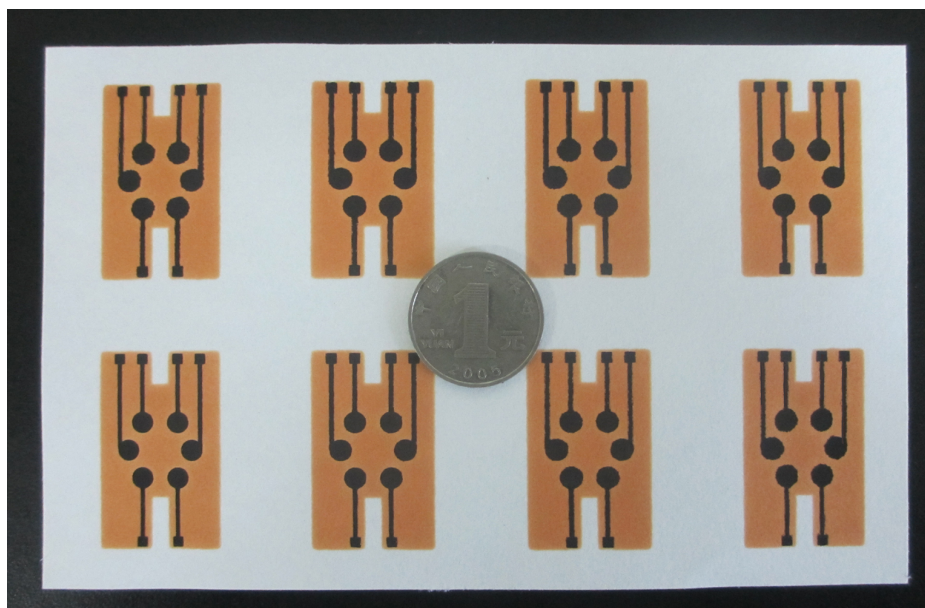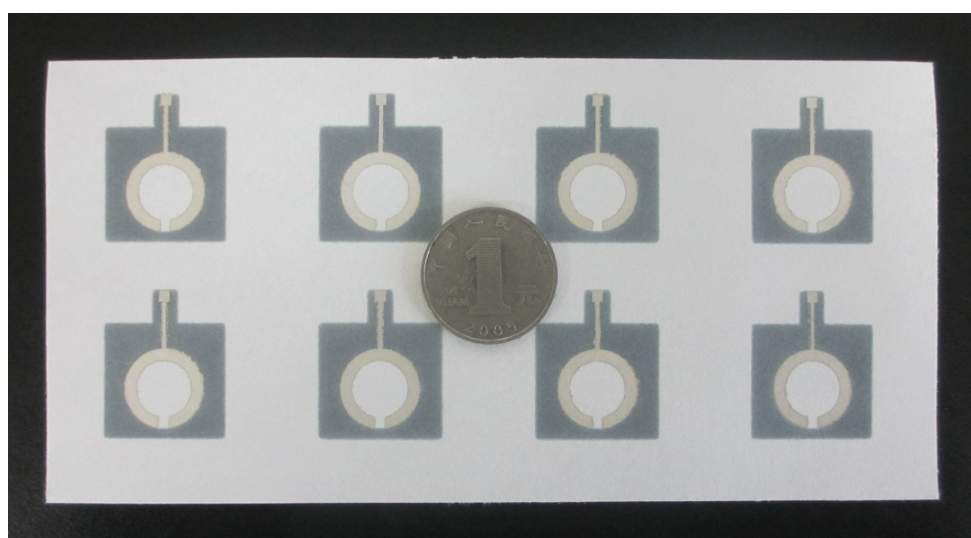
Fig. S3 Screen-printed carbon working electrodes.

Fig. S4 Screen-printed Ag/AgCl auxiliary electrodes.

Synthesis of ZnO-paper

The paper substrates used in our experiments were cut from a large piece of Whatman chromatography paper #2 with high flexibility. Prior to experiment, silver electrode was screen-printed on a piece of unmodified paper to provide a smooth surface for subsequent growth of ZnO NRs and act as a back contact. Subsequently, it was polished to and fro along one direction using an agate lapping hammer until the

surface turned smooth and shiny. After been rinsed several times by ultrapure water and dried, the larger rectangular area (36.0 mm × 20.0 mm) of these small pieces of paper were first coated with a ~100 nm thick ZnO seed layer that provides nucleation sites for the growth of ZnO NRs by pulsed laser deposition (PLD) method. For PLD experiments, a KrF excimer laser (CompexPro205, Coherent, USA) was used at a wavelength of 248 nm, with repetition rate was set at 10 Hz and deposition times of 1000. The distance from target to the front edge of the substrate was ~50 mm and the incident laser beam was at a 45° angle with respect to the ZnO target plane. During deposition, an O_2 pressure of 1.5×10^{-2} torr was attained in the chamber. The ZnO NRs were then grown from the ZnO seeds by a simple and low-cost hydrothermal process.[1] The nutrient solution used here was composed of a 30 mM 1 : 1 ratio of zinc acetate dehydrate and methenamine. The solution was fully and evenly stirred and then transferred into a Teflon reaction kettle in which the ZnO seed coated-paper substrates were suspended vertically. The reaction was carried out at 95 °C for 3.5 h in a conventional laboratory oven, and then the Teflon reaction kettle was cooled down naturally for 1.5 h before it was taken out. Subsequently, the fabricated ZnO-paper pieces were washed repeatedly with ultrapure water and baked at 80°C in a laboratory oven.

Fabrication of LEDs

To fabricate the ZnO NRs light emitting devices, PS dissolved in toluene with a concentration of 5 mg·mL^{-1} was spin-coated on the hydrothermally grown product with a rotation rate of 2000 rpm (rotations per minute) to fill in the gaps between the NRs and provide a smooth surface for subsequent thin film deposition. Oxygen plasma etching (10 Pa for 15 s) was then applied to remove PS coated on top of the ZnO NRs to expose them for junction formation with hole-conducting polymer. PEDOT:PSS was deposited subsequently on the prepared ZnO-paper by spin coating with a rotation rate of 2000 rpm.[2] Then, transparent insulating paint was applied, and exposed six circular areas for later use. This was followed by direct current sputtering of Au as the top electrode and conductive wires. The schematic diagram of the

inorganic/organic heterostructure LED was shown in Fig. 1A.

Preparation of carbon dots (CDs)

The CDs were synthesized using a simple hydrothermal method according to previous report.[3] The typical experimental procedure was described as follows: Firstly, 0.5 g gelatin was added to 25 mL water and was dissolved at 40 °C under agitation. Subsequently, the above admixture was poured into a stainless steel autoclave with a Teflon liner of 30 mL capacity and heated at 200 °C for 3.5 h. Finally, the reactor was automatically cooled to room temperature. The resulting light yellow solution was centrifuged at 16 000 rpm for 30 min to remove weight precipitate and agglomerated particles and then yielded a light brown aqueous solution of CDs for further characterization.

PEC biosensing

The paper-based ZnO NRs LED induced PEC immunoassay procedures were described below. Firstly, the photocurrent from CDs was detected by a simple digital multi-meter using the battery-triggered LED as excitation light source. To carry out the immunoreactions and target detections, 10 μL sample solution with different concentrations of CEA, CA 125 and CA 15-3 in 10.0 mM PBS (pH 7.4) were applied to the paper working zones, and allowed to incubate for 20 min at room temperature. After washing with PBS washing buffer to prevent nonspecific binding and achieve the best possible signal-to-background ratio, this prepared array could be used for PEC detection.

To demonstrate the feasibility of this paper-based ZnO NR LED induced PEC method and spatial-resolved technique strategy in multiplexed detection. The photocurrent was recorded by a simple digital multi-meter. In brief, 10.0 mL of 0.1 M PBS (pH 7.4) containing 0.1 M ascorbic acid (AA) were added into the electrochemical cell on paper-A. Then paper-A, paper-B, and paper-based LEDs were integrated with the aid of two piece of transparent glass, two binder clips and a piece of transparent polyvinylchloride (36.0 mm × 22.0 mm), as shown in Fig. 1C. Simply by changing the connection mode through the home-made multiplexed-switch, the

immunoarray (six electrodes) on paper-A could be irradiated by the battery-tiggered ZnO LED in turn.
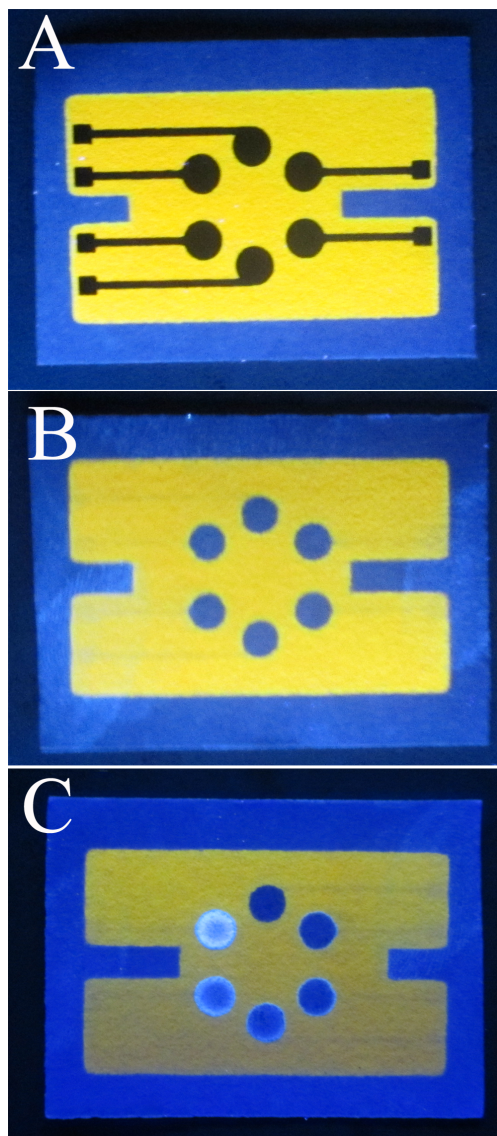

Fig. S5 Digital camera photograph of front (A) and back (B) of blank screen-printed carbon working electrodes, and (C) different concentrations of CDs modified CPWEs under UV illumination (λ_{ex} = 365 nm).

Results and discussion

Structure characterizations

In this study, ZnO NRs were grown in aqueous solution of zinc nitrate hexahydrate and methenamine ($C_6H_{12}N_4$). The reactions in solution can be described as the following formulae[4]

$$C_6H_{12}N_4 + 6H_2O \rightarrow 6HCHO + 4NH_3 \qquad (1)$$

$$NH_3 + H_2O \rightarrow NH_4^+ + OH^- \qquad (2)$$

$$Zn(NO_3)_2 \rightarrow Zn^{2+} + 2NO_3^- \qquad (3)$$

$$Zn^{2+} + 2OH^- \rightarrow Zn(OH)_2 \qquad (4)$$

$$Zn(OH)_2 \rightarrow ZnO + H_2O \qquad (5)$$
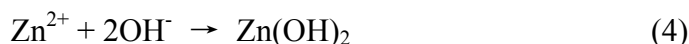
$C_6H_{12}N_4$, used in the fabrication of ZnO nanostructures, provides the OH^- to the solution. For hydrothermal method, the concen- tration of OH^- in reaction system has a great influence on the growth of ZnO NRs. So the best molar ratio between $C_6H_{12}N_4$ and $Zn(NO_3)_2$ (1 : 1)[5] was accepted for the growth of ZnO NRs on the silver coated paper substrates.

Fig. 3A showed the XRD pattern of blank paper, silver screen-printed paper, ZnO seed layer coated paper and as-prepared ZnO NRs paper. The XRD spectra of blank paper (curve a) showed the predominant characteristic peaks corresponding to cellulose (002) plane at $2\theta = 23°$ (JCPDS 03-0289).[6] As shown in curve b, except for the clear peak of cellulose, three distinct diffraction peaks at $2\theta = 38.03, 44.12$ and $64.35°$ indexed to the (111), (200) and (220) planes of face-center-cubic silver crystals could be observed, which were in good agreement with those reported in literatures,[7] suggesting that silver had been successfully deposited on paper. After coated with ZnO seed layer by PLD method, there was no other diffraction peaks appeared, indicating that a low fraction of ZnO seed layer did not affect the crystal structure of silver electrode. While, once the growth of ZnO NRs, significant XRD peaks at $2\theta = 32.06, 34.64, 36.48, 47.02, 56.50, 62.30, 66.72, 68.12$ and $69.10°$ assigned to the (100), (002), (101), (102), (110), (103), (200), (112) and (201) planes of typical hexagonal wurtzite structure ZnO (JCPD36-1451), respectively, were recorded.[8] The strong (002) peak indicates the ZnO NRs were oriented preferably along c axis, and the exhibited sharp peaks indicated that the nanostructures possess large crystalline domains as well as a high degree of crystallinity.[9] No unexpected diffraction peaks are observed in the XRD pattern, demonstrating the absence of other impurities. Furthermore, peak intensities from the bare paper (cellulose) were comparatively low

with the ZnO nanostructures grown on papers which implied the uniformity and high density of these structures as well. It could be concluded that the hexagonal-phase ZnO structures with high quality were synthesized through this simple method by low-cost hydrothermal process at low temperature.

The room temperature PL of unmodified paper, silver screen-printed paper, ZnO seed paper and ZnO NRs were examined and the result was shown in Fig. 3B. In the PL spectrum of ZnO NRs (curve d), a strong UV emission peak located at ~372 nm and a weak emission situated at ~672 nm have been observed. The UV emission peaked around 372 nm is attributed to the near band-edge transition of ZnO,[10] namely, the recombination of free excitons through an exciton-exciton collision process.[11] The strong UV emission in the PL spectrum indicates that the prepared ZnO NRs have good crystal quality. The defect-related emission at 672 nm was consistent with previous reported.[12]

Mechanism of LED device

The energy band diagrams of all materials used and PEDOT:PSS are shown in Fig. S6A. Fig. S6B shows the band diagram of the inorganic/organic heterostructure LED under positive bias. A comparison to the energy level diagram indicates that a horizontal band alignment, which is necessary for carrier injection, requires a forward potential of at least 2.4 eV: there is a 2.3 eV barrier for hole injection from PEDOT:PSS HOMO (highest occupied molecular orbit) to ZnO valence band and an additional 0.1 eV barrier between the silver and the ZnO conduction band edge.
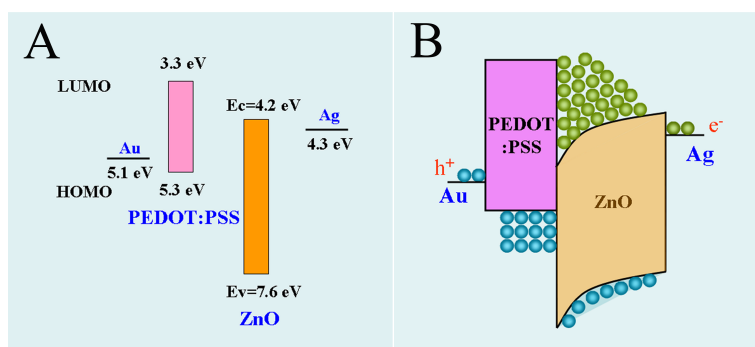

Fig. S6 (A): Energy band diagrams of ZnO, PEDOT:PSS, Ag and Au. E_C and E_V represent conduction band and valance band of ZnO, respectively. (B): Energy band diagram of the inorganic/organic heterostructure LED under a positive bias.

Meanwhile, there is a 0.2 eV barrier for hole injection from gold to PEDOT:PSS HOMO and a 0.9 eV barrier for electron injection from ZnO conduction band to PEDOT:PSS LUMO (lowest unoccupied molecular orbit). Compared with previous reported literatures,[2,13] electrons and holes could be accumulated at the ZnO/PEDOT:PSS interface under lower positive bias at the prepared device (Fig. S6B). It can be expected that a more elaborate choice of contact materials will bring about substantial reduction of these barriers or that a sequence of small energy barriers can be constructed in multilayer contacts. These refinements may eventually lead to further improvement of the luminescence onset voltage and the current densities in this type of heterojunction device.
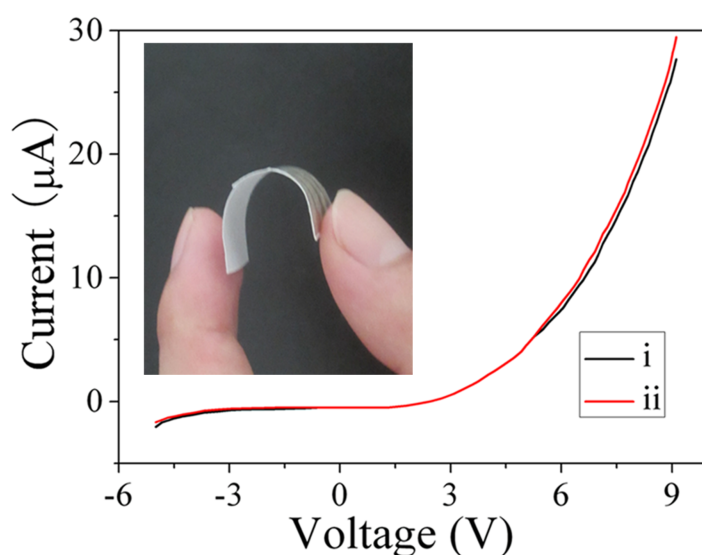

Fig. S7 The *I-V* characteristics of the paper-based ZnO NRs LED structure before (i) and after (ii) bending. The inset of (D) is its digital camera photograph, indicating its high flexibility.

Overall, this device presents an interesting alternative to organic LEDs. Because the optically active material in this hybrid structure is inorganic, stability issues may be less critical than in all-organic LEDs. The device also satisfies all of the requirements for flexible-substrate and large-area applications. Processing temperatures and procedures principally allow the use paper and the NR/PS composite appears sufficiently robust to absorb large mechanical strain. Compared to thin films, NRs

based LEDs are expected to result in an improved device performance.[14] The amplified performance in ZnO NRs based devices is presumed infect that well crystalline and well facet NRs will serve as an active and self-contained optical cavities.

Characterization of CDs

Fig. S8A shows the TEM image and the diameter distribution of CDs. It can be clearly seen that the as-synthesized CDs are uniform in size and possess a nearly spherical shape. The Gaussian fitting curve reveals that the average size of the CDs is about 2 nm, as determined by statistical analysis of more than five hundred particles by using the ImageJ soft-ware (Fig. S8B).
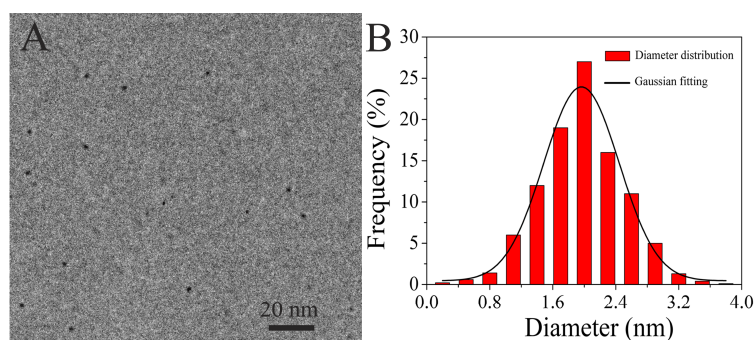

Fig. S8 TEM image (A) and the diameter distribution (B) of the CDs.

To study the optical properties of the CDs, UV-vis absorption and PL studies were carried out in detail. As illustrated in Fig. S9A, the absorption spectrum exhibits a weak broad peak around the range of 250-290 nm, which is ascribed to the typical absorption of an aromatic π system or the n-p* transition of the carbonyl.[15] The well-dispersed aqueous suspension of CDs exhibits bright blue emission under UV light, which could be easily observed with the naked eye and taken with a digital camera (inset in Fig. S9A). A broad emission centered at 430 nm was observed in the emission spectrum with an excitation wavelength at 350 nm (Fig. S9B). The peak at 350 nm appeared in the excitation spectrum reveals that the emission may be related to one kind of transition. The quantum yield measured by using quinine bisulfate as standard sample was 30.8%, which is higher than the previous report (typically <20%).[16] The higher quantum yield may be ascribed to the chemical nature and

abundant surface defects of the as-synthesized CDs.

Meanwhile, the FTIR spectrum was characterized to obtain further structural insights about the CDs, as shown in Fig. S8C. The characteristic absorption bands of O-H at 3501 cm^{-1}, the stretching vibration band of C=O at 1706 cm^{-1}, and the stretching vibration bands of C-O at 1112 and 770 cm^{-1} indicate the presence of carboxylic acid and other oxygen-containing functional groups.[15] Furthermore, the absorption around at 3038 cm^{-1} and one sharp peak at 1515 cm^{-1} are assigned to the vibration and deformation bands of N-H, suggesting the existence of amino-containing functional groups.[17] Moreover, three obvious absorption peaks at 2986, 1448 and 1324 cm^{-1} are associated with the stretching vibration C-H, C=C and C-C, suggesting the presence of alkyl and aryl groups.[18]
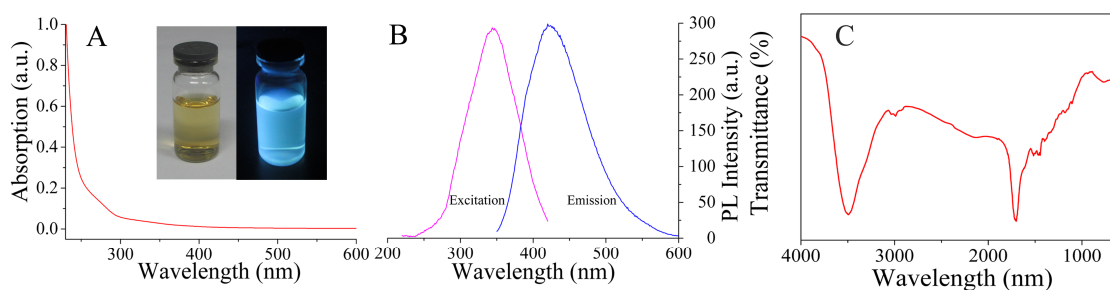

Fig. S9 (A) UV-vis absorption spectrum and (B) the PL emission and excitation spectrum the of CDs. The inset was the digital image of CDs under sunlight (left) and UV illumination (λ_{ex} = 365 nm) (right). (C): The FTIR spectrum of CDs.

Characterization of the PEC immunosensor

Previous studies have revealed that the detailed information about the immunosensor preparation and the immuno-binding on the immunosensor could be investigated by EIS.[19] Therefore, EIS (Fig. S10A) and PEC (Fig. S10B) experiments were carried out to monitor the fabrication of the immunosensor array. The impedance spectrum includes a semicircle portion and a linear portion. The semicircle portion at higher frequencies corresponds to the electron-transfer limited process, and the linear portion at lower frequencies represents the diffusion-limited process. The semicircle diameter equals the electron-transfer resistance (R_{et}), which controls the electron-transfer kinetics of the redox probe at the electrode interface. The EIS spectra
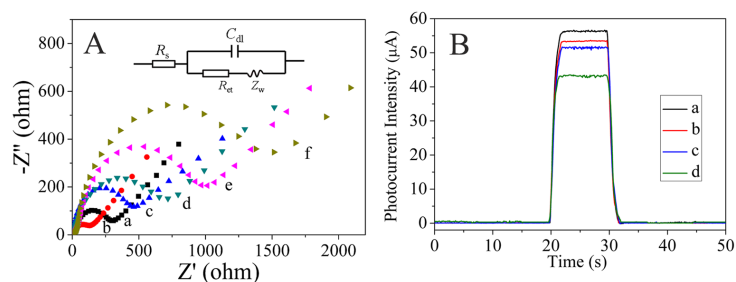
Fig. S10 (A) EIS spectra of bare CPWE (a), CPWE/CNTs-PDDA (b), CPWE/CNTs-PDDA/CDs (c), CPWE/CNTs-PDDA/CDs-Ab$_1$ before (d) and after (e) blocking with BSA, CPWE/CNTs-PDDA/CDs-Ab$_1$/CEA (f). The inset showed the equivalent circuit to fit with obtained EIS spectra. (B) Photocurrent response of CPWE/CNTs-PDDA/CDs (a), CPWE/CNTs-PDDA/CDs-Ab$_1$ before (b) and after (c) blocking with BSA, CPWE/CNTs-PDDA/CDs-Ab$_1$/CEA (d) excited by the prepared ZnO LED.

(Fig. S10A) were obtained in 5.0 mM $[Fe(CN)_6]^{3-/4-}$ solution containing 0.10 M KCl. The experimental data were fitted to a Randles equivalent circuit (the inset in Fig. S10A). In this equivalent circuit, electrolyte resistance (R_s) and Warburg element (Z_w) represent bulk properties of the electrolyte solution and diffusion of the applied redox probe in solution, respectively. Thus, they were not affected by chemical transformations occurring at the electrode/electrolyte interface. The other two components, the lipid bilayer capacitance (C_{dl}) and R_{et}, depended on the dielectric and insulating features at this interface. The change of R_{et} value was associated with the blocking behavior of the modified layer on the electrode surface, and reflected in the EIS as the change of the diameter of the semicircle at high frequencies. Its value varies when different substances were adsorbed onto the electrode surface. As seen from curve a, a relatively large resistance was obtained at the bare CPWE, which was in accordance with previous report.[20] The diameter of this semicircle was reduced in the CNTs-PDDA modified CPWE compared to the bare CPWE (curve b). These results suggest that the surface of the CNTs-PDDA modified electrode exhibited a lower electron transfer resistance and greatly increased the electron transfer rate. While, when CDs were anchored through the electrostatic interaction between positively charged PDDA and negative charged CDs, a much larger R_{et} was observed. The reason might be most likely as a consequence of the fact that the CNTs-PDDA

immobilized on the cellulose fiber surfaces played an important role similar to a conducting wire or electron conduction tunnel, which made it easier for the electron transfer to take place,[21] while the assembly of CDs into the CPWE/CNTs-PDDA partially blocked the electron transfer of the redox probe. Remarkable increase in the R_{et} value was observed after both the immobilization of Ab_1 (curve d) and blocking with bovine serum albumin (BSA) (curve e) on the surfaces of CNTs-PDDA/CDs modified cellulose fibers in CPWE, indicating that the electron-transfer kinetics of the redox probe was slow down, which testified the successful immobilization of Ab_1 and BSA blocking. Similarly, after the electrode was incubated with antigens, another kind of protein, the R_{et} increased, which were ascribed to the weak conductivity properties of biomacromolecule (curve f). These increases can entirely demonstrate the successful assembly processes on the immunosensor array.

The fabrication of the immunosensor could also be monitored by PEC experiments (Fig. S10B). As shown in curve a, the CPWE/CNTs-PDDA/CDs showed a relatively large photocurrent. While, after immobilization of the capture antibodies and BSA, the photocurrent intensity decreased (curves b and c). This could be explained by the fact that the immobilization of the proteins on the CNTs-PDDA/CDs modified electrodes generated a barrier for electron and mass transfer and significantly slowed down the diffusion rate of electrons donor (AA) to the surface of CDs for reaction with the photogenerated holes and resulted in the decrease in the photocurrent intensity.[22] After the as-obtained biosensor was incubated with the corresponding antigen (curve d), the photocurrent further decreased. The decrease in the photocurrent was ascribed to the increase in steric hindrances for the diffusion of AA due to the formation of the immuno-complex.[23] Control experiments, which were carried out with the biosensor incubated with PBS solution without antigen, showed no change in photocurrent intensity. This further proved that the photocurrent decrease was due to the immunoreaction. On the basis of the photocurrent decrease due to the formation of the immunocomplex, a multiplexed PEC immunosensor array was achieved.

Evaluation of cross-reactivity and cross-talk

As shown in Fig. 4B, the photocurrent intensity at WE3 was much higher than that at WE1, and WE2 for the detection of 0.1 ng·mL^{-1} CEA (line B). When the CEA concentration increased to 0.5 ng·mL^{-1} (WE6), the photocurrent intensity decreased while no obvious signal changes were observed at WE4 and WE5 electrodes. This indicated that there was no obvious cross-talk among the examined electrodes. The relative standard deviations (RSDs) of the average photocurrent intensity obtained at any one of the electrodes for tetradic measurements were less than 5%. Furthermore, the same phenomenon was observed for the independent detection of CA 125 and CA-153 (lines C and D). Therefore, the interfering response resulting from the signal substances diffusion between the adjacent immunosensors was almost eliminated, as has frequently been encountered in some electrochemical immunosensor arrays.[24] Also, since each immunosensor only responded to its corresponding tracer antibody, the cross-reactivity between each capture antibody and its noncognate antibodies was negligible. As desired, PEC response (line D) did not decreased even though the addition of other antigens. Apart from that, the photocurrent signals from different immunosensors were triggered by prepared paper-based LEDs in turn with aid of the homemade multiplexed-switch. This novel strategy also avoided the cross-talk resulting from current-diffusion. Furthermore, compared with other reported PEC immunosensors for the detection of CEA and CA 15-3 (Table S1), wider linear range and lower detection limit were achieved without an external light source.

Table S1. Analytical performances of various PEC immunosensors.

Targets	Linear range (ng·mL^{-1}) or (U·mL^{-1})	LOD (pg·mL^{-1}) or (mU·mL^{-1})	References
CEA	0.05-20	10	25
CEA	0.005-20	1.8	This work
CA 15-3	0.02-70	7.1	21
CA 15-3	0.01-50	3.8	This work

To elevate the coefficient of variation of intra-assay, immunosensors belonging to

the same batch were used to detect three different concentrations of each antigen. The variation coefficient of five times parallel test were 6.4%, 5.9% and 5.3% for 0.1, 0.5, 1 ng·mL^{-1} CEA; 6.7%, 6.1% and 5.7% for 0.1, 1, 10 U·mL^{-1} CA 125; 6.1%, 5.6% and 5.2% for 0.1, 1, 10 U·mL^{-1} CA 15-3, respectively. When using different batches of immunosensors, the coefficient of variation was investigated at same condition, and the results were 9.0%, 8.5% and 7.8% for CEA; 9.5%, 8.9% and 8.6% for CA 125; 8.7%, 8.5% and 8.2% for CA 15-3, respectively. Thus, the immunosensor array showed a desirable reproducibility.

Additionally, long-term storage stability of the proposed immunosensors array was also investigated. The immunosensor array stored at 4°C for 20 days showed that the steady-state Δphotocurrent for the detection of 0.1 ng·mL^{-1} CEA, 0.50 U·mL^{-1} CA 125 and 0.50 U·mL^{-1} CA 15-3, were 97.5%, 97.1% and 96.7% of the initial steady-state Δphotocurrent, respectively. And the average decrease value of Δphotocurrent was less than 5.6%, 6.3% and 7.1% than that of freshly prepared immunosensor, when the resulting immunosensors were stored for 40 days. Consequently, the proposed immunoassay system possessed perfect stabilization in practical applications.

Application in analysis of serum samples

In the tumorous process, increased levels of tumor markers in human serum are significantly associated in patients with certain tumor or carcinoma. Thus, the detection of tumor marker levels in serum is of importance which can give information of the disease stage, the grade of metastasis and the recidivism of tumors.[26] To evaluate the analytical reliability and application potential of the designed immunoassay method, the assay results of CEA, CA 125 and CA 15-3 in clinical serum samples (provided by Shandong Cancer Hospital) using the proposed method were compared with the reference values (the results were provided by Shandong Tumor Hospital, China) obtained by commercial available Electrochemiluminescent Analyzer (ROCHE E601, Switzerland).[27] When the levels of tumor markers were over calibration ranges, serum samples were appropriately diluted with 0.01 M PBS (pH 7.4) prior to the assay. The experimental results were

summarized in Table S2. The RSDs were 3.75-7.03%, 4.37-6.19% and 4.11-7.74%
for CEA, CA 125 and CA 15-3, respectively. No significant differences were
encountered, thereby revealing a good correlation between the two methods.

Table S2. Assay results of clinical serum samples using the proposed and reference methods.

Sample No.	Proposed method ($ng \cdot mL^{-1}$ or $U \cdot mL^{-1}$)[a]			Reference method ($ng \cdot mL^{-1}$ or $U \cdot mL^{-1}$)[a]			RSD (%)[a]		
	CEA	CA 125	CA 15-3	CEA	CA 125	CA 15-3	CEA	CA 125	CA 15-3
1	1.68	7.86	13.19	1.49	7.78	13.28	4.69	6.03	4.11
2	0.85	15.37	20.28	0.97	15.24	20.37	3.75	5.72	7.74
3	1.12	19.43	28.47	1.26	19.67	28.61	7.03	6.19	6.59
4	2.03	27.14	9.72	1.97	26.89	9.57	5.67	4.37	5.84
5	2.51	10.95	13.55	2.70	11.12	13.62	4.96	5.82	5.67

[a]The average value of six successive determinations.

References

1 (a) Y. Qiu, H.Q. Zhang, L.Z. Hu, D.C. Yang, L.N. Wang, B. Wang, J.Y. Ji, G.Q. Liu, X. Liu, J.F. Lin, F. Li, S.J. Han, *Nanoscale*, 2012, **4**, 6568; (b) Z. Wang, X. Zhan, Y. Wang, S. Muhammad, Y. Huang, J. He, *Nanoscale*, 2012, **4**, 2678.

2 C.Y. Chang, F.C. Tsao, C.J. Pan, G.C. Chi, H.T. Wang, J.J. Chen, F. Ren, D.P. Norton, S.J. Pearton, K.H. Chen, L.C. Chen, *Appl. Phys. Lett.*, 2006, **88**, 173503.

3 Q.H. Liang, W.J. Ma, Y. Shi, Z. Li, X.M. Yang, *Carbon*, 2013, **60**, 421.

4.   Z.F. Liu, E. Lie, J. Ya, Y. Xin, *Appl. Surf. Sci.*, 2009, **255**, 6415.

5. H.H. Guo, J.Z. Zhou, Z.H. Lin, *Electrochem. Commun.*, 2008, **10**, 146.

6 A. Manekkathodi, M.Y. Lu, C.W. Wang, L.J. Chen, *Adv. Mater.*, 2010, **22**, 4059.

7 (a) Q.L. Huang, H. Chen, L.L. Xu, D.Q. Lu, L.L. Tang, L.T. Jin, Z.A. Xu, W. Zhang, *Biosens. Bioelectron.*, 2013, **45**, 292; (b) L.M. Chang, Y. Ding, X. Li, *Biosens. Bioelectron.*, 2013, **50**, 106.

8 H.J. Zhang, B.A. Chen, H. Jiang, C.L. Wang, H.P. Wang, X.M. Wang, *Biomaterials*, 2011, **32**, 1906.

9 X.J. Feng, L. Feng, M.H. Jin, J. Zhai, L. Jiang, D.B. Zhu, *J. Am. Chem. Soc.*, 2004, **126**, 62.

10 C. Li, G.J. Fang, F.H. Su, G.H. Li, X.G. Wu, X.Z. Zhao, *Nanotechnology*, 2006, **17**, 3740.

11 Y.C. Kong, D.P. Yu, B. Zhang, W. Fang, S.Q. Feng, *Appl. Phys. Lett.*, 2001, **78**, 407.

12 X.W. Sun, J.Z. Huang, J.X. Wang, Z.Xu, Nano Lett. 2008, **8**, 1219.

13 R. Ko1nenkamp, R.C. Word, M. Godinez, Nano Lett., 2005, **5**, 2005.

14 Y.Y. Lin, C.W. Chen, W.C. Yen, W.F. Su, C.H. Ku, J.J. Wu, *Appl. Phys. Lett.*, 2008, **92**, 233301.

15 C. Zhu, J. Zhai, S. Dong, *Chem. Commun.*, 2012, **48**, 9367.

16 (a) X. Jia, J. Li, E. Wang, Nanoscale, 2012, **4**, 5572; (b) C.W. Lai, Y.H. Hsiao, Y.K. Peng, P.T. Chou, *J. Mater. Chem.*, 2012, **22**, 14403; (c) Z. Zhang, J. Hao, J. Zhang, B. Zhang, J. Tang, *RSC Adv.*, 2012, **2**, 8599.

17 (a) Z. Ma, H. Ming, H. Huang, Y. Liu, Z.H Kang, *New J. Chem.*, 2012, **36**, 861; (b) P.C. Hsu, H.T. Chang, *Chem. Commun.*, 2012, **48**, 3984.

18 S. Liu, J. Tian, L. Wang, Y. Zhang, X. Qin, Y. Luo, A.M. Asiri, A.O. Al-Youbi, X. Sun, *Adv. Mater.*, 2012, **24**, 2037.

19 (a) G.F. Jie, L. Wang, S.S. Zhang, *Chem. Eur. J.*, 2011, **17**, 641; (b) J. Zhou, D.P. Tang, L. Hou, Y.L. Cui, H.F. Chen, G.N. Chen, *Anal. Chim. Acta*, 2012, **751**, 52; (c) G.H. Yang, J.T. Cao, L.L. Li, R.K. Rana, J.J. Zhu, *Carbon*, 2013, **51**, 124.

20 G.F. Jie, L.L. Li, C. Chen, J. Xuan, J.J. Zhu, *Biosens. Bioelectron.*, 2009, **24**, 3352.

21 P.P. Wang, L. Ge, S.G. Ge, J.H. Yu, M. Yan, J.D. Huang, *Chem. Commun.*, 2013, **49**, 3294.

22 Q. Kang, L.X. Yang, Y.F. Chen, S.L. Luo, L.F. Wen, Q.Y. Cai, S.Z. Yao, *Anal. Chem.*, 2010, **82**, 9749.

23 Y.R. An, L.L. Tang, X.L. Jiang, H. Chen, M.C. Yang, L.T. Jin, S.P. Zhang, C.G. Wang, W. Zhang, *Chem. Eur. J.*, 2010, **16**, 14439.

24 F. Leng, G.S. Lai, F. Yan, H.X. Ju, *Anal. Chim. Acta*, 2010, **666**, 97.

25 W.W. Tu, W.J. Wang, J.P. Lei, S.Y. Deng, H.X. Ju, *Chem. Commun.*, 2012, **48**, 6535.

26 F.Y. Kong, B.Y. Xu, J.J. Xu, H.Y. Chen, *Biosens. Bioelectron.*, 2013, **39**, 177.

27 Y. Zhang, W.J. Dai, F. Liu, L. Li, M. Li, S.G. Ge, M. Yan, J.H. Yu, *Anal. Bioanal. Chem.*, 2013, **405**, 4921.